Gas Processing Journal

Vol. 10, No. 1, 2022, pp. 67 - 84
http://gpj.ui.ac.ir

Research Paper

Techno-Economic and Exergetic Analysis and Optimization of Integrated MED- RO Desalination System in the Genaveh Combined Cycle Power Plant

Mohammad Reza Abedi [1], Gholamreza Salehi[2], Masoud Torabi Azad [1*], Mohammad Hasan Khosgoftar Manesh[3,4], Hossein Fallahsohi[1]

[1] Energy Systems Engineering Group, Faculty of Marine Science, North Tehran Branch, Islamic Azad University, Tehran, Iran
[2] Mechanical Engineering Group, Faculty of Engineering, Central Tehran Branch, Islamic Azad University, Tehran, Iran
[3] Energy, Environmental and Biological Systems Research Lab (EEBRlab), Division of Thermal Sciences and Energy Systems, Department of Mechanical Engineering, Faculty of Technology & Engineering, University of Qom, Qom, Iran
[4] Center of Environmental Research, University of Qom, Iran

Received: 2021-10-01 Revised: 2022-03-31 Accepted: 2022-04-30

Abstract: Hybrid power and desalinated water generation systems with two Multi-Effect Distillation (MED) technologies and Reverse Osmosis (RO) are investigated for a combined-cycle power plant in this study. The generated steam enters MED from the low-pressure section of the Heat Recovery Steam Generator (HRSG) in the hybrid system. Seawater is divided into two sections after entering the MED condenser – one part is fed into MED and its process. The other is rejected after cooling in the condenser and turns back to the sea. A reverse osmotic desalination system is implemented in this study. In the present combined cycles, steam generated in the Low Pressure (LP) section enters the steam turbine. To reduce the generated power and increase desalinated water in MED and RO, exergy analysis and cycle optimization are required. The system is simulated and verified based on the available data on the model power plant. The results showed that by selecting 43 optimization parameters and applying constraints like acidification temperature, the integrated cycle's exergy efficiency could be raised by 50%. Under this condition, the water price is calculated to be 1.16 $/m3. Under hybrid conditions of the design power and freshwater cogeneration system, the present design's efficiency without optimization and its final cost is 48.8% and approximately 1.2 $/m3.

keywords: Hybrid desalination system, MED, RO, combined cycle, economic analysis, exergy.

Abbreviations

MED	Multi-Effect Distillation	ERC	Energy recovery cycle
RO	Reverse Osmosis	TVC	with thermal vapor compression
CCPP	combined-cycle power plant	TTR	total tariff revenue
HRSG	Heat Recovery Steam Generator	AFUDC	allowance for funds used during construction
LP	Low Pressure	LRD	research and development
MSF	multi-stage flash	ISO	International Standards Organization
TDS	Total dissolved water	WC	working capital
UPC	unit production cost	SUC	startup cost
ONSC	on-site costs	CRF	Capital recovery factor
TTD	Total temperature difference	FCI	fixed capital investment

* **Corresponding Author.**
Authors' Email Address: [1] M. R. Abedi (abedi.tavanir@yahoo.com), **[2] M. Torabi,** (torabi_us@yahoo.com), **[3] M. R. Abedi,** (abedi.tavanir@yahoo.com)' **[4] M. H. Khoshgoftar Manesh,** (mh.khoshgoftar@gmail.com), **[5] H. Fallahsohi,** (hossein.fallahsohi@gmail.com)

http://dx.doi.org/10.22108/GPJ.2022.130805.1108

Parameters			
L	latent heat of vaporization	Q	water produced
H	elevation	y	flash fraction
Phot	hot pressure drop	n	number of effects
U	velocity at the compressor outlet	J_w	flow rate of passing water
T_B	inlet air temperature	J_s	salt flow rate from the membrane
T_C	outlet air temperature	F	mass flow rate of supply water
ρ	inlet air density	D	desalinated water flow rate
$\overline{\lambda}$	fuel to air molar ratio	A	Area

1. Introduction

Water resources are a source of concern in Iran. Only 2.5% of the world's water is desalinated, and as low as 3% of this is available to use. The rest of this water is reserved as ice or underground water. Compared to other countries, Iran is in a generally concerning condition, especially when it comes to water per capita. Also, the average annual growth of electricity consumption is twice as great (Khoshgoftar Manesh *et al.*, 2021) as its average global consumption rate. The average annual growth of electricity consumption has been 8% in the past 30 years, and the electricity facilities get twice bigger every ten years. Consequently, water and electricity capacities must be promoted.

Looking at the most common approaches in the world, the most applicable and main methods of seawater desalination in medium and high volumes are reverse osmotic (RO), multi-effect distillation (MED), and multi-stage flash (MSF), among which RO is the most popular(Shenvi, Isloor, and Ismail, 2015). However, suppose a thermal power resource is utilized. In that case, there is access to seawater, and the water volume and temperature and concentration of salt and total dissolved solids (TDS) are high enough, MSF and MED will be more economical. The technology for the production of materials used in RO is not yet common in Iran. Still, when there is additional electricity in the network, the RO method can be used to optimize the related capacities supplying the basic load. MED+RO combined cycle is suggested.

Although the MSF technology has contributed the most to the (sea) water desalination, new developments in the MED technology and its advantages compared to MSF have flourished in its market. Accordingly, in many new plans for simultaneous water and power generation on the Persian Gulf's southern coasts, MED (instead of MSF) is combined with thermal power plants. This method is characterized by its low sensitivity to the inlet water quality compared to other methods, capability to work with the inlet water with diverse characteristics, lower electricity consumption rate, and higher quality of water produced (TDS<10 ppm), making it suitable for different industrial applications. The ability to be designed in higher capacities of 70000 m^3/day and the potential of MED-TVC manufacturing technology in Iran are other important benefits of MED technology. RO systems have wide ranges of capacity, but high expenses of electricity, the maintenance of membrane change (every 4-5 years), high sensitivity to inlet water quality, and additional expenses of inlet water pretreatment are some drawbacks.

(Al-Hallaj *et al.*, 2004) presented a novel fuel cell desalination unit system's conceptual design. They proposed two states for the combined cycle. First, one combined fuel cell with the RO method and one combined fuel cell with a thermal desalination unit. The results showed that the desalination unit's energy requirement was reduced by as much as 80% by preheating inlet water to the RO system using the fuel cell's outlet gas. Also, the fuel cell-thermal desalination unit system's efficiency was increased by 5.6% concerning the independent systems of fuel cell and water desalination units. It was found that, based on the type of the desalination unit, the fuel cell can be added more efficiently to the system where the generated electricity and dissipated heat can be used to produce desalinated water. (Lisbona, Uche and Serra, 2005) investigated a hybrid system where fuel cell was integrated with MSF and RO desalination systems. The fuel cell supplied the Ro system's electricity demand and recovered outlet gas before preheating RO and MSF supply water. The results were investigated for two types of fuel cell, solid oxide, and Molten Carbonate Fuel cells. These results showed that the efficiency was 95% for SOFC and 78% for MCFC.

Investigating a MED system with a thermal vapor compressor to optimize the maximum accessible outlet rate (GOR) and reduce consumed power, (Kamali *et al.*, 2008) developed a computer program and applied it to a sample of desalinated water at the capacity of 1500 m^3/day. Moreover, they showed that thermodynamic optimization for the constant area's heat transfer surface increased GOR and the system's total capacity. (Kamali and Mohebinia, 2008) presented a model and algorithms for optimizing a MED_TVC desalination unit in Qeshm Island based on an evaporator, a thermo-compressor, an ejector, and finally, an entire desalination cycle. (Skiborowski *et al.*, 2012) optimized two MED systems with a progressive inlet and RO combined with a power plant unit using mixed-integer non-linear programming (MINLP).

Various literature has applied genetic algorithms for the optimization of different desalination units. For instance, (Najafi *et al.*,

2014) implemented a multi-objective genetic algorithm for the optimization of an MSF distillation unit integrated with a steam turbine-solid oxide fuel cell. The target function parameters included exergy efficiency and total cost ratio to minimize the environmental effects (environmental pollution) and maximize exergy efficiency after thermodynamic and numerical simulation by the multi-objective genetic algorithm. (Shahandeh, Ivakpour and Kasiri, 2014) implemented a genetic algorithm to optimize the inlet and outlet of a heat-integrated distillation column using thermodynamic equations for a multi-parameter target function. (Esfahani and Yoo, 2013) used a genetic algorithm to promote a gas turbine system and desalination unit by optimizing important thermodynamic parameters such as flow rate and compressor temperature for the highest exergy efficiency. A thermo-economic model based on exergy analysis and nuclear plant energy with a high-pressure water reactor and a MED-TVC desalination system was studied. The optimization was based on a genetic algorithm with 16 parameters in the target function to minimize the system's production expenses, including desalinated water and electricity generation. A similar work (Sayyaadi, Saffari, and Mahmoodian, 2010) studied the optimization of the MED-TVC desalination unit's thermo-economic model. They presented a complete explanation of fuel production in the MED-TVC system's exergy analysis. The economic model was based on total tariff revenue (TTR). The optimization problem consisted of six parameters in the target function, and appropriate constraints were applied. The optimization process was used by the genetic algorithm, and the results proved to be economically appropriate. Additional steam of electricity system networks that produce industrial steam processes in different steps can be used to run desalination units. A genetic algorithm has been used by (Manesh *et al.*, 2013) to determine an optimal combination of a MED-RO desalination system. Furthermore, a linear parabolic collector has been optimized by genetic algorithms in several studies. (Silva *et al.*, 2014) optimized a solar parabolic collector thermo-economically using a genetic algorithm. The design parameters included the number of collectors in each row, the number of rows, the space occupied by each collector row, and the reservoir's volume. (Gomar, Heidary and Davoudi, 2011) analyzed different desalination units thermo-economically under Asaluyeh climatic conditions. (El Saie, El Saie and El Gabry, 2003) studied a simultaneous cycle of double-objective power generation of gas and steam turbines with desalination units in Sharmo-al-shaikh with capacities of 500MW and 25 MIGD from a thermo-economic point of view in 2002. (El-Nashar, 2001) presented an optimal, thermo-economical design for water-electricity simultaneous generation systems. (Mokhtari, Ahmadisedigh and Ebrahimi, 2016) supplied desalinated water for Miarkla (north Iran) using an RO system. In this study, 4000 m^3/day is required to supply desalinated water for 12000 people after 20 years. Energy, exergy, economic analyses, and environmental effects are considered in designing the power plant and solar farm. This means that RO, power plants and solar systems are designed based on water demand. Previous studies have been done based on the solar system and its generated power (Mokhtari, Bidi and Gholinejad, 2014).

(Rahimi and Alibabaee, 2021) compared different scenarios for the combined generation of power and water production in Iran. Multi-objective optimization Qeshm power plant combined with water production studied by (Vazini Modabber and Khoshgoftar Manesh, 2019). Water can be produced in a greenhouse by seawater in the south of Iran (Salehi, Ahmadpour, and Khoshnazar, 2011). Multi-generation of power, steam, and Freshwater in studded and designed by (Ghiasi *et al.*, 2022). Energy, exergy, exergoeconomic, exergoenvironment, exergoeconomic, and exergoenvironmental assessment of an innovative quadruple combined cycle coupled with magneto hydrodynamic generator has been performed with five different organic fluids by (Esmaeilzadehazimi *et al.*, 2021). The results indicated that the R141b with overall energy and exergy efficiency of 15.25 and 58.05%, respectively, had the best thermodynamic and exergy performance with the least amount of total costs using this fluid. (Seckin, 2020) investigated the operational parameters of an innovative combined cycle of ERC and Kalina Cycle. The maximum overall energy and exergy efficiency results were obtained when R290 and R134a are used. (Khoshgoftar Manesh *et al.*, 2021) performed dynamic conventional and advanced exergy, exergoeconomic, and environmental assessment of a combined solar city gate station. All evaluations are performed with a 1-h time-step and are considered precisely.

As mentioned above, in previous research, the integration of desalination plants and power plants has been discussed. But a hybrid compound has been less commonly studied. This paper aims to integrate MED and RO desalination systems with a combined cycle power plant to generate power and fresh water simultaneously. Techno-Economical, exrgetic analysis, and optimization have been done for the proposed system. In this regard, Genevah combined cycle power plant has been considered.

2. Process Description

In this study, a Combined Cycle Power Plant has been investigated. The scope consists of a

combined cycle block consisting of 2 gas units, each with the capacity of 162 megawatts and a steam turbine with the capacity of 160 MW in ISO conditions (overall 484 MW), and a steam division including two boilers (HRSG), each with the capacity of 310 tons of steam and ACC cooling system. The cycle proposed in this study is shown in Figure 1.

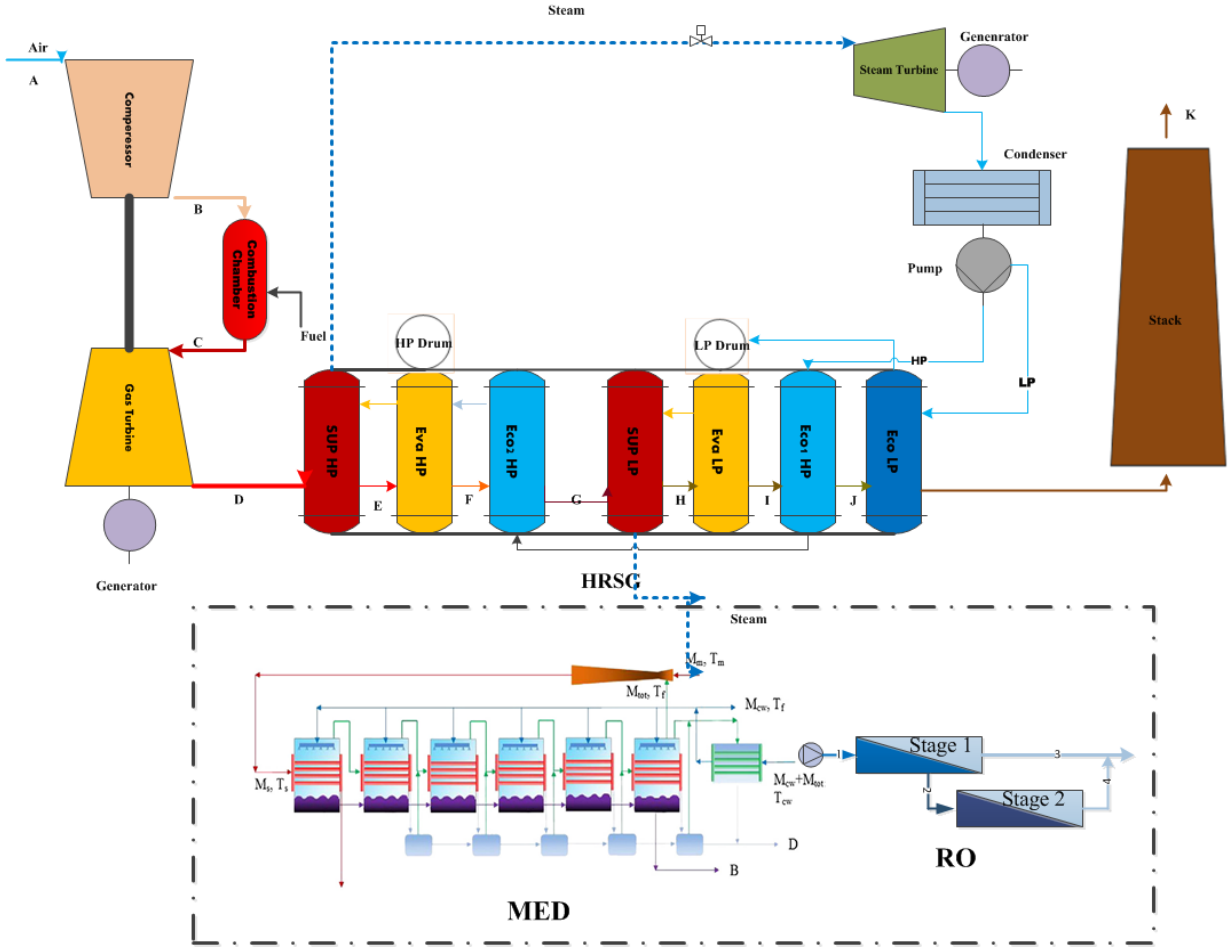

Figure 1. A schematic representation of the proposed cycle

3. Thermodynamic Modeling

3-1- Gas turbine

A gas turbine V94.2 is simulated under site conditions in Hormozgan (Southern Iran) and close to the Persian Gulf. Table 1 shows the required inputs for the gas turbine cycle.

Table 1. Input data for the simulation of the gas turbine (Esmaieli et al., 2013; Mokhtari, Esmaieli, and Hajabdollahi, 2016)

Parameter	unit	value
Elevation	M	20
Average annual ambient temperature	°C	27
Average annual humidity	%	68
Compressor pressure ratio	-	11.1
Inlet temperature to gas turbine under full load	°C	1060
Compressor isentropic efficiency	%	85.5
Gas turbine isentropic efficiency	m	20

The simulation of gas turbines has been the main subject of some articles (Esmaieli *et al.*, 2013; Mokhtari, Esmaieli, and Hajabdollahi, 2016). Here, only the differences between the proposed model and the previous ones are presented. The compressor inlet pressure is determined by Eq. (1).

$$P_{atm} = \frac{(760 \times (1\text{-}226 \times 10^{-7} \times H)^{5.25})}{735} \quad (1)$$

where H is the elevation and P_{atm} is expressed in bars. Air humidity is also taken into account in these equations. Looking into the calculations, this parameter influences the water molar fraction.

In addition to the cold pressure drop calculated by (Lefebvre and Ballal, 2010), the hot pressure drop is also considered:

$$\Delta P_{hot} = 0.5 \rho U^2 \left(\frac{T_C}{T_B} - 1 \right) \quad (2)$$

The substantial pressure drop occurring in the combustion chamber is a product of the combustion process and depends on the velocity

at the compressor outlet (U) in m/s, inlet air temperature TB and outlet air temperature TC from the combustion chamber, and inlet air density ρ in kg/m3.

The combustion equation, each component's fraction, and finally energy equation are presented in Eq. (3-10):

$$\lambda C_x H_y + \left[x_{N_2} N_2 + x_{O_2} O_2 + x_{H_2O} H_2O + x_{CO_2} CO_2 + x_{Ar} Ar\right] \rightarrow y_{N_2} N_2 + y_{O_2} O_2 + y_{H_2O} H_2O + y_{CO_2} CO_2 + y_{CO} CO + y_{NO} NO + y_{Ar} Ar \quad (3)$$

$$y_{CO_2} = \lambda x + x_{CO_2} - y_{Co} \quad (4)$$

$$y_{H_2O} = \frac{\lambda y}{2} + x_{CO_2} \quad (5)$$

$$y_{Ar} = x_{Ar} \quad (6)$$

$$y_{N_2} = x_{N_2} - \frac{y_{Co}}{2} \quad (7)$$

$$y_{O_2} = x_{O_2} + \frac{y_{Co} y_{No}}{2} - \lambda x - \frac{\lambda y}{4} \quad (8)$$

$$\bar{h}_{air} + \bar{\lambda}\bar{h}_{fuel} + \bar{s}\bar{h}_{steam} = \bar{h}_{gas}\left(1 + \bar{\lambda}\right) + 0.02 \times \mathrm{LHV} \times \bar{\lambda} \quad (9)$$

$$\bar{\lambda} = \frac{x_{O_2}\Delta\bar{h}_{O_2} + x_{N_2}\Delta\bar{h}_{N_2} + x_{CO_2}\Delta\bar{h}_{CO_2} + x_{H_2O}\left(\bar{h}_{H_2O,T_D} - \bar{h}_{H_2O,T_C}\right)}{\bar{h}_f + x\bar{h}_{O_2,T_D} + y\bar{h}_{O_2,T_D}/4 - x\bar{h}_{CO_2,T_D} - y\bar{h}_{H_2O,T_D}/2 - 0.02 \times \mathrm{LHV}} \quad (10)$$

Eq. (11) calculates $\bar{\lambda}$ using its definition (fuel to air molar ratio):

$$\bar{\lambda} = \frac{\dot{m}_f}{\dot{m}_{air}} \times \frac{M_{air}}{M_f} \quad (11)$$

X and y are the amount of carbon and hydrogen in fuel and are calculated based on a combination of power plant consumed fuel. Eq. (4) to (8) are derived from balancing chemical equations. On the other hand, the enthalpy of the combustion products and the air is calculated $\bar{h} = \sum_{i=1}^{N} x_i \bar{h}_i$. So, Eq. (10) is derived from combining this equation with Eq. (9) and its simplification. Gas turbine simulation is expressed according to Ref. (Kaviri, Jaafar, and Lazim, 2012).

3-2- HRSG design

Solving energy equations is required in HRSG design. By writing energy equations for each component, including economizer (Eq. (12)), evaporator (Eq. (13)), super-heater (Eq. (14)), and approach (Eq. (15)) and pinch (Eq. (16)) axillary equations, the thermodynamic parameters can be calculated. These equations are presented in Table 2 and solved in a system of equations for each pressure surface (Esfahani and Yoo, 2013) (Mokhtari, Ahmadisedigh, and Ebrahimi, 2016) (Ansari, Sayyaadi and Amidpour, 2010).

Table 2. Energy equations of each pressure surface in HRSG

Equation

$$\dot{m}_g Cp_g \left(T_{g,o} - T_{g,i}\right) = \dot{m}_f \left(h_{w,o} - h_{w,i}\right) \quad (12)$$

$$\dot{m}_g Cp_g \left(T_{g,o} - T_{g,i}\right) = \dot{m}_f \left[\left(h_v - h_{w,o}\right) + BD\left(h_1 - h_{w,o}\right)\right] \quad (13)$$

$$\dot{m}_g Cp_g \left(T_{g,o} - T_{g,i}\right) = \dot{m}_f \left(h_{s,o} - h_{s,i}\right) \quad (14)$$

$$T_{ap} = T_{sat} - T_{w,o} \quad (15)$$

$$T_{pp} = T_{g,o,eva} - T_{sat} \quad (16)$$

As Q and logarithmic temperature gradient are definite, thermal surfaces are calculated as below (Ganapathy, 2002):

$$A = \frac{Q_f}{U \Delta T_{LM}} \quad (17)$$

where U is obtained from Eq. (18):

$$\frac{1}{U} = \frac{1}{\eta_o h_o} + f_o + \frac{A_i}{A_{wi}} f_i + \frac{A_i}{A_{wi}} \frac{1}{h_i} + \frac{A_i}{A_w} \frac{d_o \ln\left(\frac{d_o}{d_i}\right)}{2K_m} \quad (18)$$

where the areas are calculated from equations in (Ganapathy, 2002). Considering the type of flow inside the channel and assuming triangular adjustments, the heat transfer coefficient can be obtained for the outside part of the finned channels (Ganapathy, 2002; Esmaieli *et al.*, 2013; Mokhtari, Esmaieli and Hajabdollahi, 2016).

The pressure drop for two-phase flow for water is calculated from Eq. (19)-(22): average pressure drop of water, frictional pressure drop, gravitational pressure drop, and pressure drop resulting from acceleration.

$$\Delta P_{ave} = \Delta P_f + \Delta P_{gr} + \Delta P_a \quad (19)$$

$$\Delta P_f = 0.82 \times 10^{-15} \times \frac{v_f f_m l_e G^2 r_3}{14.5 d_i} \quad (20)$$

$$\Delta P_{gr} = 142.359 \times 10^{-10} \times \frac{N_w l_e r_4}{14.5 v_f} \quad (21)$$

$$\Delta P_a = 0.34074 \times 10^{-16} \times \frac{v_f G^2 r_2}{14.7} \quad (22)$$

Following equations are applied to find these parameters for gas:

$$\Delta P_g = Z \times \frac{G_g{}^2 N_r}{500 \times \rho_g} \quad (23)$$

$$\rho_g = \frac{640.8}{1.8T_{g,ave} + 32 + 460} \quad (24)$$

$$T_{g,ave} = \frac{T_{g,i} + T_{g,o}}{2} \quad (25)$$

$$G_g = \frac{\dot{M}_g}{N_w (P - A_o) L} \quad (26)$$

$$A_o = d_o + 2n_f t_f h_f \quad (27)$$

3-3- MED design

In a MED system design, the equations are categorized into three groups. The first group consists of conservation equations and the generated water flow rate (Table 3). The second group includes energy equations (Table 4), and the third is related to the area required for heat transfer and heat transfer coefficients (Table 5).

Table 3. Mass balance, GOR, and desalinated water production

Equation	Title
$B_1 = F_1 - D_1$	Mass balance in the first effect
$B_i = F_i + B_{i-1} - D_i + \left[y_{i-1} \left(D_r + \sum_{j=1}^{i-2} D_j \right) \right] - \left[(i-1) F_{i-1} y_{i-1} \right]$	Mass balance from the second to the nth effect
$D_{Con} = D_n - D_r + \left[y_n \left(D_r + \sum_{i=1}^{n-1} D_i \right) \right]$	Mass balance in the condenser
$D = \left[(1-y_n) \left(D_r + \sum_{i=1}^{n-1} D_i \right) \right] - \left[y_{n-1} \left(D_r + \sum_{i=1}^{n-2} D_i \right) \right] - \left[y_{n-2} \left(D_r + \sum_{i=1}^{n-3} D_i \right) \right] - \left[y_{n-3} \left(D_r + \sum_{i=1}^{n-4} D_i \right) \right] - \left[y_{n-4} \left(D_r + \sum_{i=1}^{n-5} D_i \right) \right] - \left(y_{n-5} . D_r \right) + D_{con} . y_6$	Mass balance in the condensation tank
$C_{sw} F_1 = C_{B_1} B_1$	Salt balance in the first effect
$C_{sw} F_i + \left(C_{B_{i-1}} B_{i-1} \right) = C_{B_i} B_i$	Salt balance from the second to the nth effect
$GOR = \frac{D}{S}$	
$Q = 86.4.D$	Desalinated water production rate

Table 4. Energy balance equations

Equation	Title
$D_1 L_1 + \left(F_1 C_p \left(T_1 - T_{f1} \right) \right) = \left(Dr + S \right) L_0$	Energy balance in the first effect
$D_i L_i + \left(F_i C_p \left(T_i - T_{fi} \right) \right) = \left(D_{i-1} L_{i-1} \right) + \left(y_{i-1} \left(D_r + \sum_{i=1}^{i-2} D_i \right) L_{i-1} \right) - (i-1) \left(F_{i-1} y_{i-1} L_{i-1} \right) + \left(B_{i-1} C \left(T_{i-1} - T_i \right) \right)$	Energy balance from the second to the nth effect

Table 5. Thermal area equations and heat transfer coefficients

Equation	Title
$A_{e1}=\frac{(Dr+S)L_0}{U_{e1}.(T_{0c}-T_1)}$	Area of the first effect
$A_{ej}=\frac{\left(\left(y_{i-1}\left(D_r+\sum_{i=1}^{i-2}D_i\right)+D_{i-1}\right)-(i-1)(F_i y_{i-1})\right)L_{i-1}}{U_{ei}.(T_{v_{i-1}}-T_i)}$	Area of the second effect and subsequent ones
$A_{H_i}=\frac{(i.F_i.C.(T_{f_i}-T_{f_{i+1}}))}{U_{H_i}.LMTD_{H_n}}$	Area of pre-heater 1 to n-1
$A_{H_n}=\frac{(n.F_n.(T_{f_n}-T_f))}{U_{H_i}.LMTD_{H_n}}$	Area of pre-heater n
$A_{Con}=\frac{\left(\left(y_n\left(D_r+\sum_{i=1}^{n-1}D_j\right)+D_{con}\right)-(i-1)(F_i y_{i-1})\right)L_n}{U_{con}.LMTD_{con}}$	Area of heat transfer condenser
$U_{e_1}=1.9394+(1.40562\times10^{-3})T_{0c}-(2.07525\times10^{-5})T_{0c}^{\ 2}+(2.3186\times10^{-6})T_{0c}^{\ 3}$	Heat transfer coefficient of the first effect
$U_{e_i}=1.9394+(1.40562\times10^{-3})T_{v_{i-1}}-(2.07525\times10^{-5})T_{v_{i-1}}^{\ 2}+(2.3186\times10^{-6})T_{v_{i-1}}^{\ 3}$	Heat transfer coefficient of the second to the n^{th} effect
$U_{H_i}=14.1825162+(0.011381865)T_{v_i}+0.013381501T_{f_{i+1}}$	Heat transfer coefficient of pre-heater to n-2^{th}
$U_{H_{n-1}}=14.1825162+(0.011381865)T_{v_{n-1}}+0.013381501T_f$	Heat transfer coefficient of pre-heater n-1
$U_{Con}=1.6175+(1.537\times10^{-4})T_{v_n}-(1.825\times10^{-4})T_{v_n}^{\ 2}+(8.026\times10^{-8})T_{v0}^{\ 3}$	Heat transfer coefficient of the condenser

where A is the area under heat transfer (m^2), B is the flow rate (kg/s), C is the concentration (ppm), D is the desalinated water flow rate (kg/s), F is the mass flow rate of supply water (kg/s), Q is the water produced (m^3/day), S is the injecting steam flow rate (kg/s), T is the temperature (°C), L is the latent heat of vaporization, y is the flash fraction, and n is the number of effects.

3-4- RO system design

The RO system design consists of several stages, comprehensively explained in (Mokhtari, Bidi, and Gholinejad, 2014). Here, only the main equations for one element are discussed and presented in Table 6.

Eq. (1)-(8) state flow rate of passing water (J_w) and salt (J_s) from the membrane and based on mass transfer equations (kg/m^2.s). The average velocity of passing flow is found in a row (3). Salt concentration in the product is determined from row (4). Also, because of the mass transfer process's concentration polarization, the salt concentration of the membrane wall for supply water (C_w) is calculated from row (5) and based on the film theory. According to the conservation equation, rows (6) and (7) are used for water and row (8) for salt, where A and B are water and salt permeability coefficients, respectively.

Table 6. Main equations for simulating one RO element

Equation	
$J_w = A \times TCF \left[\left(P_f - P_p - \frac{\Delta P_f}{2} \right) - \left(\pi_w - \pi_p \right) \right] \times 10^6$	1
$J_s = B \left(C_w - C_p \right)$	2
$V_w = \frac{J_w + J_s}{\rho_p}$	3
$C_p = \frac{J_s}{V_w} \times 1000$	4
$C_w = C_p + \left(\frac{C_f + C_b}{2} - C_p \right) e^{\frac{V_w}{k}}$	5
$Q_p = V_w S_m$	6
$Q_B = Q_F - Q_P$	7
$C_B = \frac{Q_F C_F - Q_P C_P}{Q_B}$	8

4. Economic analysis

Total capital investment is the sum of fixed capital investment (FCI), startup cost (SUC), working capital (WC), licensing, research and development (LRD), and allowance for funds used during construction (AFUDC).

$$\mathrm{TCI} = \mathrm{FCI} + \mathrm{SUC} + \mathrm{WC} + \mathrm{LRD} + \mathrm{AFUDC} \quad (28)$$

There are different methods to state equipment costs in terms of design parameters. But, this study focuses on the cost functions of RO (Esfahani et al., 2012), MED (Mokhtari, Ahmadisedigh, and Ebrahimi, 2016), and other components (Bejan and Tsatsaronis, 1996). Zk is the equipment purchase cost for the kth component, and N is the number of working hours per year. The capital recovery factor (CRF), which depends on the interest rate and equipment estimated life, is:

$$\mathrm{CRF} = \frac{\mathrm{i}(1+\mathrm{i})^{\mathrm{n}}}{(1+\mathrm{i})^{\mathrm{n}} - 1} \quad (29)$$

Where n is the power plant service life, and i is the interest factor. By having equipment purchase costs and on-site costs (ONSC), the total capital investment is estimated. RO and MED system operating costs are calculated (Mokhtari, Ahmadisedigh, and Ameri, 2017) (Esfahani et al., 2012). The annual operating cost is:

$$AOC_{Total} = AOC_{Other} + AOC_{MED} + AOC_{RO} \quad (30)$$

Normalized total cost is:

$$TAC = {TCI}/{CRF} + AOC_{Total} \quad (31)$$

The unit production cost of desalinated water is obtained as follows:

$$UPC = \frac{TAC}{24 \times Q_p \times 365} \quad (32)$$

Input parameters in this economic modeling are introduced in Table 7.

Table 7. The input parameters for the economic analysis

parameter	*value*
System total capacity factor (f_c)	***0.9***
Inflation	***10***
System operating time	***20***
Power price,c_{el}) \$/kWh(	***0.08***

5. Computational Algorithm

A computational algorithm for analysis and multi-objective optimization has been demonstrated in Figure.2. As indicated, thermophysical properties for each stream and also a thermodynamic simulation of the gas cycle. heat recovery section and MED-RO desalination have been performed in MATLAB. Then, economic analysis and thermoeconomic analysis have been done using developed code in MATLAB. In the final step. Multi-objective optimization through a Genetic Algorithm has been carried out. The objective functions are minimization of produced water final cost for the MED and RO systems (\$/m^3) and exergy efficiency of the overall cycle. Table 8 shows decision variables, the lower and upper limits. Table 8. Indicates the decision variables and its lower and higher limit.

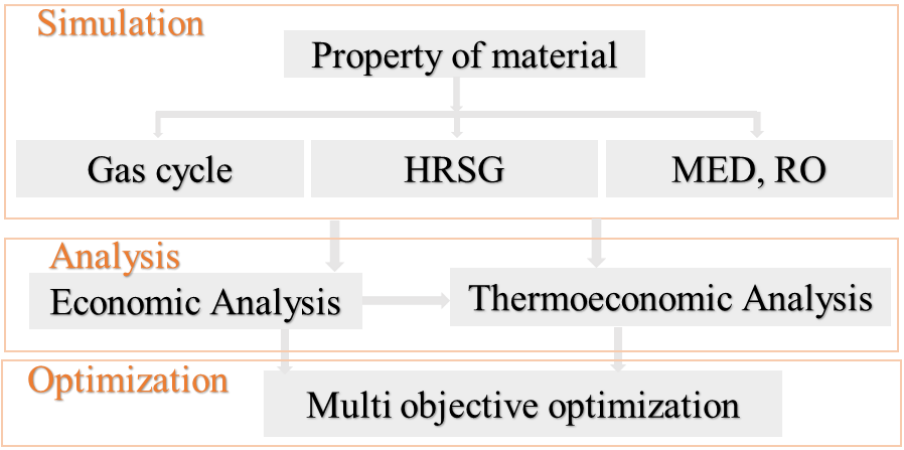

Figure 2. Computational algorithm for analysis and multi-objective optimization

Table 8. Decsion variables and their lower and higher limit

No.	Parameter	Lower limit	Upper limit
1	LP vapor pressure (bars)	5	14
2	LP vapor temperature (°C)	150	250
3	Condenser pressure (bars)	0.08	0.14
4	Number of pipe rows in MED condenser	5	90
5	External diameter of MED condenser pipes (mm)	20	80
6	Condenser pipe length (m)	2	5
7	Number of passages and effects in the condenser	2	5
8	Condenser width (m)	3	5
9	Condenser height (m)	0.5	5
10	Number of effects in MED	3	8
11	Temperature gradient of each effect (°C)	2	6
12	Number of pipe rows in MED condenser	5	90
13	Pipe thickness of each effect in MED	0.7	1.8
14	External diameter of each MED effect (mm)	20	80
15	Pipe length of each MED effect (m)	2	5
16	Internal diameter of economizer exchanger (mm)	20	100
17	Internal diameter of evaporator exchanger (mm)	20	100
18	Internal diameter of superheater exchanger (mm)	20	100
19	Pitch of economizer exchanger pipes (mm)	35	285
20	Pitch of evaporator exchanger pipes (mm)	35	285
21	Pitch of superheater exchanger pipes (mm)	35	285
22	Height of economizer exchanger fins (mm)	13	25
23	Height of evaporator exchanger fins (mm)	13	25
24	Height of superheater exchanger fins (mm)	13	25
25	The thickness of economizer exchanger fins (mm)	0.9	3
26	The thickness of evaporator exchanger fins (mm)	0.9	3
27	Height of economizer exchanger fins (mm)	0.9	3
28	Length of fined pipes of economizer exchanger (m)	10	30
29	Length of fined pipes of evaporator exchanger (m)	10	30

30	Length of fined pipes of superheater exchanger (m)	10	30
31	Thickness of economizer exchanger fin (mm)	2	8
32	Thickness of evaporator exchanger fin (mm)	2	8
33	Thickness of superheater exchanger fin (mm)	2	8
34	Density of economizer fin (No/m)	50	275
35	Density of evaporate fin (No/m)	50	275
36	Density of superheater fin (No/m)	50	275
37	supply pressure of RO system (MPa)	4	8
38	Suggested recovery for RO system design	0.4	0.98
39	Number of membranes in each PV	4	8
40	low pressure pinch temperature (°C)	5	50
41	high pressure pinch temperature (°C)	5	50
42	low pressure approach temperature (°C)	5	50
43	high pressure approach temperature (°C)	5	50

6. Verification

The simulation results are compared with Thermoflex software, as shown in Tables 9 and 10. As indicated, the simulation results are in good agreement with the Thermoflex simulation.

The results of the MED verification are shown in Table 11.

Table 9. The comparison between data and results of the simulation for the gas cycle

	Unit	Thermoflex	Simulation	Error
T_B	℃	360.23	362.57	0.65
T_D	℃	546	546.02	0.0
m_f	kg/s	8.0	7.6787	0.92
η	%	33.43	30.7957	1.76

Table 10. The comparison between data and results of the simulation for the gas cycle

	Unit	Thermoflex	Simulation	Error
h_1	kg/kj	206.77	203.06	1.8
h_4	kg/kj	667.86	666.4525	0.21
h_7	kg/kj	2907.9	2832.9	2.6
h_8	kg/kj	668.83	672.9670	0.62
h_{13}	kg/kj	3436.35	3437.6	0.03
T_E	℃	603.94	594.17	1.6
T_F	℃	557.55	562.13	0.82
T_G	℃	494.23	497.13	0.58
T_H	℃	317.38	310.36	2.21
T_I	℃	244.87	241.15	1.23
T_K	℃	242.36	239.4141	1.2
T_M	℃	182.44	179.85	1.42
T_L	℃	201.94	201.66	0.13
T_P	℃	106.51	106.31	0.19
T_{17}	℃	48	48.04	0.083
T_1	℃	49	48.542	0.93

Table 11. MED verification results

parameter	Simulation results	Reference data (Hosseini, Amidpour and Shakib, 2012)	Error (%)
Desalinated water production (m^3/day)	1317	1300	1.3

The reverse osmotic system is verified by (Du *et al.*, 2014). This system is designed in one stage with 33 pressure pipes. There are three membrane elements of SW30HR-380 for each pipe organized in a parallel way. The supply water flow rate and concentration are 214.8 m^3/h and 7410 TDS. As shown in Table 12, the highest error value is found to be 0.13 for this sample. A similar permeability coefficient for all salts (Du *et al.*, 2014) is supposed to be the reason for this low error, especially in water concentration.

Table 12. verification with reference (Du et al., 2014)

parameter	Results in [32]	simulation	Error (%)
Concentration of salt in produced water in step 1 (ppm)	30.0	30.56	1.8
(m3/h) Produced water in step 1	97.1	97.06	0.041
Input supply pressure (MPa)	4.4	3.8	13.6
Water treatment (%)	45.2	45.2	0

7. Results

Pinch temperature is an important item to consider in designing a heat recovery boiler. In this section, sensitivity analysis is applied to high-pressure pinch temperatures. With an increase in high-pressure pinch temperature, the results show that heat absorption in the low-pressure part and the produced vapor volume are reduced. Consequently, vapor production rises. So, it can be inferred that pinch temperature is a parameter to increase vapor production in the desalination section. Variations in steam flow rates in different pinch temperatures are plotted in Figure 3. On the other hand, the steam flow rate directly influences power generation. The generated power is illustrated in Figure 4.

According to Figure 5, as the heat recovery boiler is designed for the CCPP cycle and considered stand-alone Power Plant data is implemented in CCPP+MED and CCPP+MED+RO cycles, the exergy efficiency is reduced LP steam supplied for MED must have better features to increase exergy efficiency. In this sensitivity analysis, the recovery boiler requires additional design in a CCPP+MED+RO system to promote hybrid system efficiency. Accordingly, pinch temperature is an important design parameter, playing a significant role in steam generation in heat recovery boilers and power and desalinated water generation. So, this parameter must be taken into account in the optimization process.

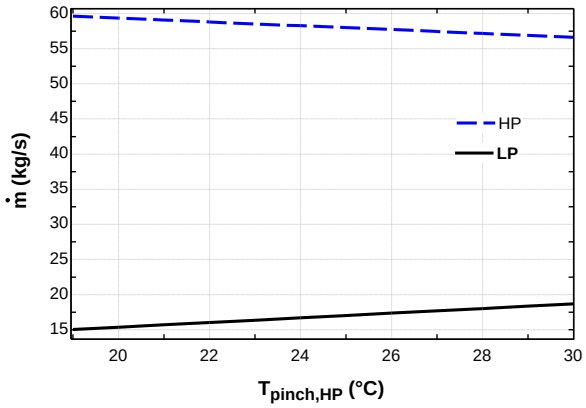

Figure 3. Variations in steam flow rate concerning different pinch temperatures

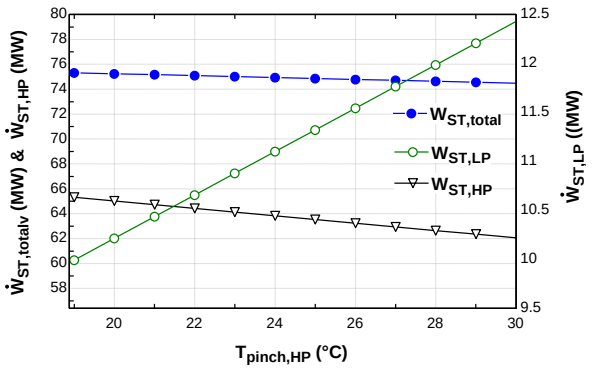

Figure 4. Variations in generated power concerning different pinch temperatures

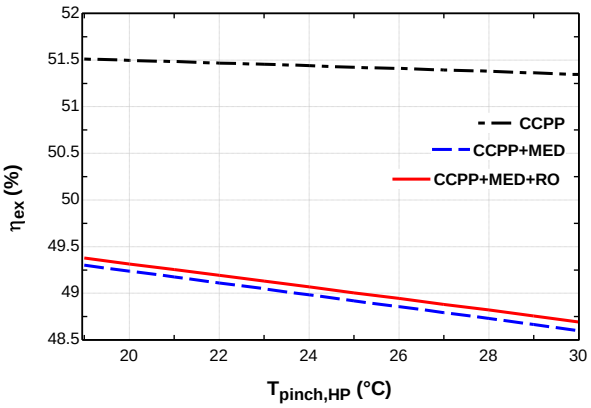

Figure 5. The exergy efficiency of each state of the combined cycle concerning variations in pinch temperature

5-1- Water desalination hybrid system

The curves presented in this section show a perfect integration of the proposed code. Therefore, it can cover ambient and pinch temperature effects, which influence gas and steam turbines on both desalination systems.

Another important parameter in the proposed system is the produced desalinated water. This

system consists of two membrane desalination systems or RO and MED. Figure 6 shows the results of daily desalination in the hybrid system. As indicated, RO produces more desalinated water than MED because it desalinates the entire water rejected from the MED condenser, which is substantially high in amount. RO pump power is high enough for this volume of desalination. The generated pressure in this pump is 67 bars, and the desalinated water has a quality of 447 ppm (<1000ppm) in this system, which is perfectly appropriate for consumption. With a rise in ambient temperature and a fall in steam flow rate, the amount of water entering the sea to keep the MED system in a constant performance ratio reduces. This will decrease the produced and rejected water, which will affect the desalinated water flow rate of the RO system. In addition, the variations in the RO-MED system pump power concerning pinch temperature have been demonstrated in Figure 7.

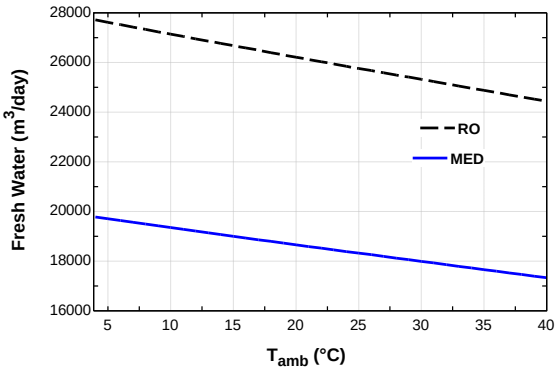

Figure 6. The desalinated water flow rate in the MED+RO hybrid system

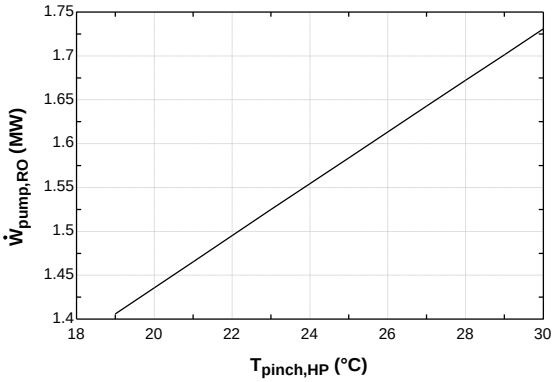

Figure 7. Variations in the RO-MED system pump power concerning pinch temperature

An essential analysis for these two systems is the exergy analysis. Exergy destruction in MED is more than that in the RO system (Figure 8), which can be attributed to the different processes occurring in these two systems. There is a big difference between hot and cold flows in the MED system, which results in more entropy production and exergy destruction. As the ambient temperature goes up, the rejected flow rate goes down. Subsequently, the flow rate of the RO input water and its consumed power and desalinated water flow rate all diminish.

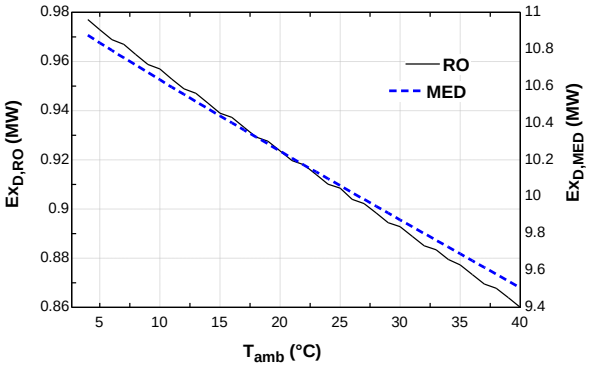

Figure 8. Variations in exergy destruction in hybrid systems (MED+RO) concerning ambient temperature

As indicated in Figure 9, a system with more desalinated water produced has a lower final cost. In conclusion, the generated power price in RO systems is quite constant and experiences a little ascending trend while it is less in MED systems. Looking at the decrease in the rejected flow rate, less desalinated water is generated, and the final cost goes up. This analysis assumes that the RO system's power is supplied from the power plant itself, and no additional cost is presumed for this item. So, the only effective parameter is the desalinated water reduction in the RO system. A decline in thermal areas for a constant performance ratio reduces the final cost for MED in a thermal system.

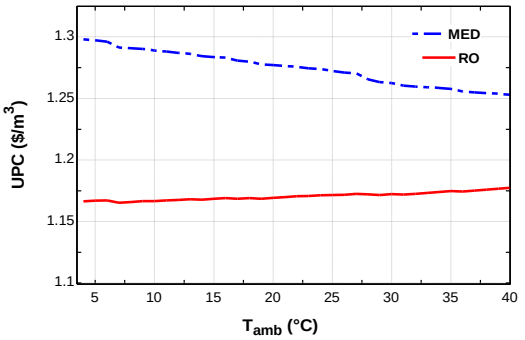

Figure 9. Produced water final cost for the MED and RO systems

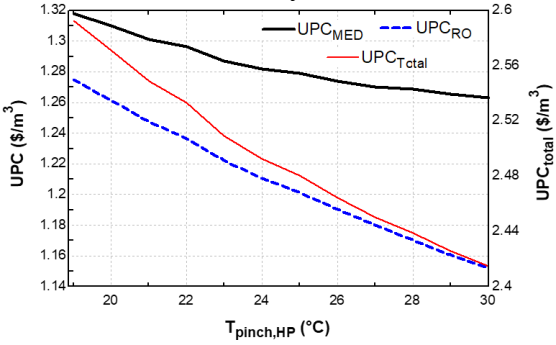

Figure 10. Variations in the produced and desalinated water final price in the MED+RO hybrid system

Figure 10 demonstrates the variations in the produced and desalinated water's final price for high-pressure pinch temperature. This figure proves the effect of pinch temperature on the steam flow rate in Figure 2. As the pinch temperature goes up, an increase in the steam produced in LP results in a higher flow rate of the desalinated water produced and reduces the final cost. In different states of a combined cycle, the variations in exergy efficiency regarding ambient temperature are recognized (Figure 11). This sensitivity analysis shows that the heat recovery boiler in the considered Power Plant is not beneficial for a hybrid desalination system and must be designed again. If the generated steam enters the steam turbine, the combined cycle's exergy efficiency will increase versus the states of desalinated water production.

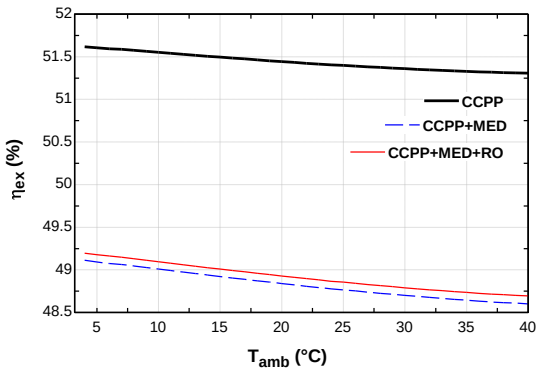

Figure 11. Variations in the system's exergy efficiency in different states

5-2- Analyzing CCPP+MED+RO system

Figure 12 indicates the result of the CCPP+MED+RO system simulation for this power plant. At a temperature of 27°C, which is the average ambient temperature in this area, the volumetric flow rate of air changes from 510 to 497 kg/s. Regarding the pressure ratio of 12.5 in the compressor and polytropic and isentropic processes, the temperature rises to 404°C. After injecting natural gas at a flow rate of 8.3 kg/s, the combustion products' temperature increases to 1100°C. Because of the high airflow rate, the fraction of oxygen combinations in the combustion products considerably decreases from 21% to 13%. The net generated power (145 MW) of the combustion products moves toward a heat recovery boiler with a temperature of 542°C. It creates two pressure surfaces of 90 bars of 520°C and 8.5 bars of 233°C and exits the chimney at 144°C. The generated steam in the high-pressure section causes a power of 63 MW. Then, the steam produced in the condenser's high-pressure part is condensed at 48°C and enters the pump. Supplying LP and HP pressures, the pump increases the pressure to 21 and 13 bars to overcome the passage pressure drop. The generated steam enters MED consisting of 5 stages in addition to a condensing stage.

It is assuming TTD= 3.3°C, the pressure is obtained in each step. The seawater of 48000 ppm enters the system and is divided into two parts. One part is fed into each step, and the desalinated water flow rate will get to 643 m3/h. The rest (2588 m3/h) enters the RO system. By consuming 1.8 MW, the pump creates a pressure of 67 bars (6.8 MPa). This will end in desalinated water production in two stages. First, producing desalinated water of 319 ppm concentration at a flow rate of 998 m3/h, and second, desalinated water of 2745 ppm concentration at a flow rate of 67 m3/h. Mixing these two steps produced desalinated water of 417 ppm concentration at a flow rate of 1066 m3/h.

The final results are presented in Table 13. According to the results, the internal consumption of the plant is almost 3 MW. This system has produced 1730 m^3/h of desalinated water, 60% of which is created in the RO system and the rest in the MED system.

Most of the exergy destruction occurs in the combustion chamber and is equal to 160 MW or 64% of the total exergy destruction (Figure 13). Heat recovery boiler (14%) and MED (approximately 4%) are in the following ranks (Figure 14).

Most of the exergy destruction occurs in the combustion chamber and is equal to 160 MW or 64% of the total exergy destruction (Figure 13). Heat recovery boiler (14%) and MED (approximately 4%) are in the following ranks (Figure 14).

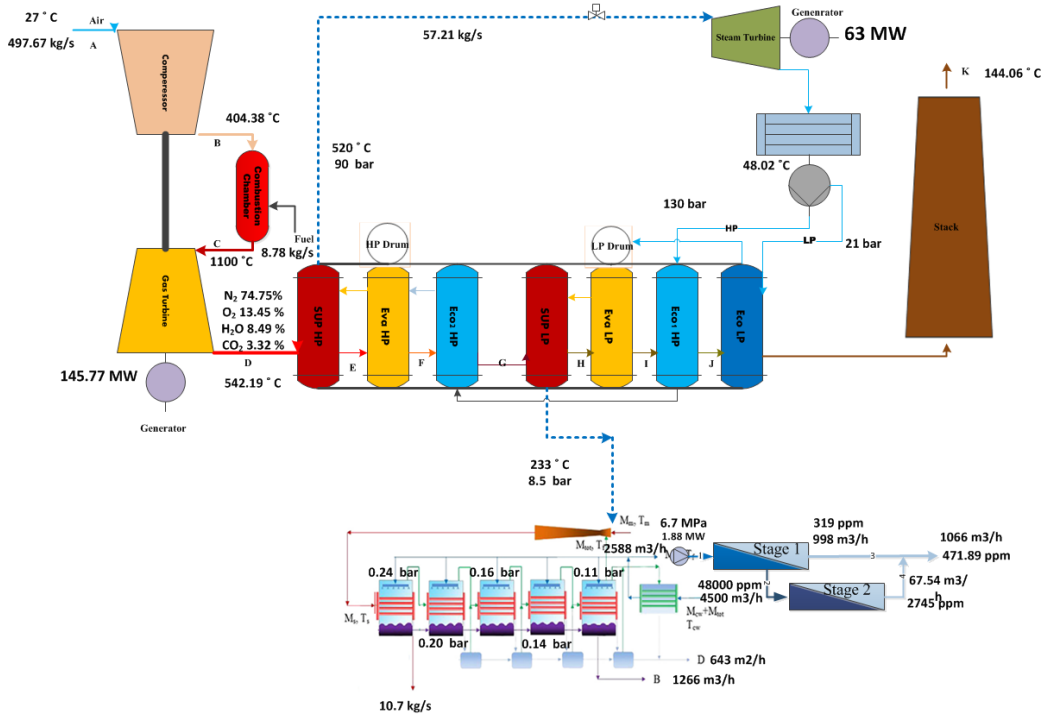

Figure 12. The simulation results of proposed power and freshwater cogeneration plant

Table 13. The important parameters of power and freshwater cogeneration plant

parameter	value
Cycle exergy efficiency (%)	48.8
Total desalinated water produced (m3/h)	1730
The final concentration of desalinated water in RO/MED	471.0
Generated power in one block (MW)	208.7777
Net generated power in one block (MW)	205.39
The final cost of heat recovery boiler (M$)	21.05
Produced water price in MED ($/m3)	1.27
Produced water price in RO ($/m3)	1.17
Total exergy destruction of cycle (MW)	251.06

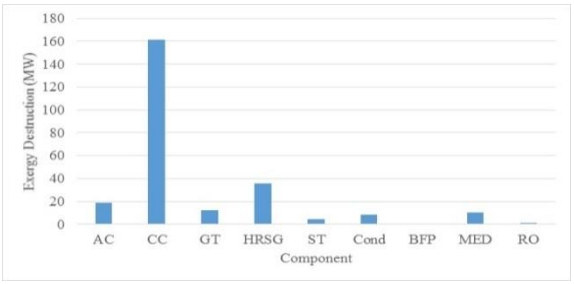

Figure 13. The exergy destruction for the individual cycle components

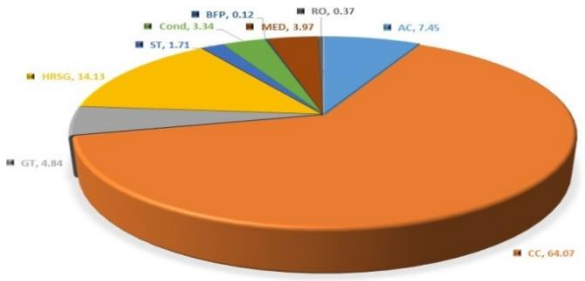

Figure 14. The exergy destruction of each component

5-3-Hybrid system optimization

As indicated in sensitivity and cycle analysis, the heat recovery boiler is not designed according to the mentioned hybrid system's thermodynamic second law. The hybrid system diminishes exergy efficiency. Subsequently, this section aims at improving exergy efficiency and reducing the final cost of the produced desalinated water. In this regard, systems added in the hybrid scheme to CCPP in addition to the heat recovery boiler need to be redesigned and improved. The optimization scenario is schematically presented in Figure 15. The gas turbine's HP and outlet conditions are supposed to be constant, and LP is assumed to be variable. Accordingly, HRSG is designed. The design parameters of MED and RO are also analyzed. Decision-making parameters in the optimized range and their optimal values are given in Table 13.

Following the implementation of genetic algorithms and the defined decision-making parameters, the results of optimization are

introduced in Figure 16. The optimization results are shown by a ray curve, which divides solution space into possible and impossible/inaccessible areas. The boundary consists of optimal points where the results are optimized. Each point in this system that is close to the ideal point (the highest exergy efficiency and lowest final cost) has the best point among ray curve points. Based on the desalinated water price and system total exergy efficiency, each point of this curve can be selected and evaluated. If the best points are chosen according to the approach introduced in Figure 16, it can be seen that the main vapor pressure and temperature have been selected in an equal sequence.

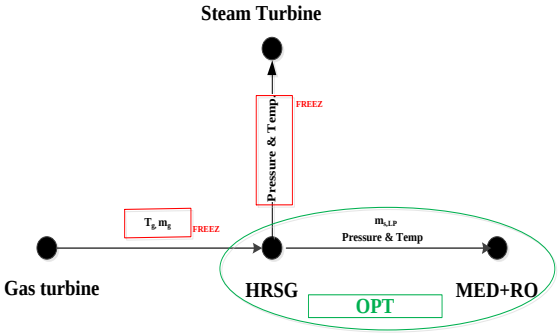

Figure 15. The schematic representation of the CCPP+MED+RO combined cycle optimization scenario

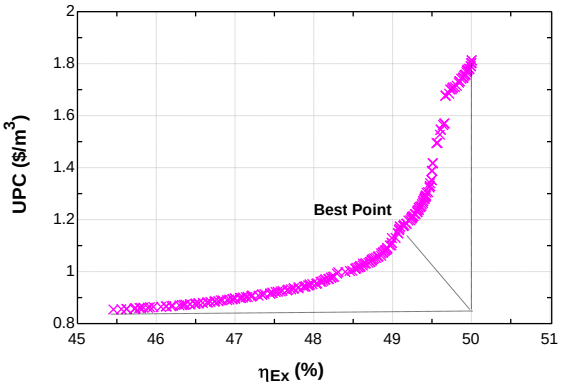

Figure 16. The hybrid system optimization curve

Table 13. The decision-making parameters and optimization results

No.	Parameter	Lower limit	Higher limit	Optimal values
1	LP vapor pressure (bars)	5	14	7.80
2	LP vapor temperature (°C)	150	250	12.49
3	Condenser pressure (bars)	0.08	0.14	0.084
4	Number of pipe rows in MED condenser	5	90	41
5	External diameter of MED condenser pipes (mm)	20	80	40.10
6	Condenser pipe length (m)	2	5	4.81
7	Number of passages and effects in the condenser	2	5	5
8	Condenser width (m)	3	5	4.03
9	Condenser height (m)	0.5	5	1.77
10	Number of effects in MED	3	8	5
11	Temperature gradient of each effect (°C)	2	6	5.95
12	Number of pipe rows in MED condenser	5	90	49
13	Pipe thickness of each effect in MED	0.7	1.8	1.30
14	External diameter of each MED effect (mm)	20	80	57.31
15	Pipe length of each MED effect (m)	2	5	4.35
16	Internal diameter of economizer exchanger (mm)	20	100	40.33
17	Internal diameter of evaporator exchanger (mm)	20	100	57.27
18	Internal diameter of superheater exchanger (mm)	20	100	61.95
19	Pitch of economizer exchanger pipes (mm)	35	285	94.65
20	Pitch of evaporator exchanger pipes (mm)	35	285	107.88
21	Pitch of superheater exchanger pipes (mm)	35	285	140.54
22	Height of economizer exchanger fins (mm)	13	25	15.85
23	Height of evaporator exchanger fins (mm)	13	25	16.39
24	Height of superheater exchanger fins (mm)	13	25	19.06

25	The thickness of economizer exchanger fins (mm)	0.9	3	1.48
26	The thickness of evaporator exchanger fins (mm)	0.9	3	1.94
27	Height of economizer exchanger fins (mm)	0.9	3	2.23
28	Length of fined pipes of economizer exchanger (m)	10	30	17.56
29	Length of fined pipes of evaporator exchanger (m)	10	30	21.46
30	Length of fined pipes of superheater exchanger (m)	10	30	21.24
31	Thickness of economizer exchanger fin (mm)	2	8	5.35
32	Thickness of evaporator exchanger fin (mm)	2	8	3.34
33	Thickness of superheater exchanger fin (mm)	2	8	2.95
34	Density of economizer fin (No/m)	50	275	131.30
35	Density of evaporate fin (No/m)	50	275	154.16
36	Density of superheater fin (No/m)	50	275	116.92
37	supply pressure of RO system (MPa)	4	8	7.62
38	Suggested recovery for RO system design	0.4	0.98	0.80
39	Number of membranes in each PV	4	8	6.0
40	low pressure pinch temperature (°C)	5	50	20.14
41	high pressure pinch temperature (°C)	5	50	8.76
42	low pressure approach temperature (°C)	5	50	21.05
43	high pressure approach temperature (°C)	5	50	15.05

According to optimal data, efficiency has increased by as much as 50%, and the final cost has decreased to 1.16 $/m^3. In conclusion, based on the governing equations and genetic algorithm, the efficiency and final cost have been improved.

8. Conclusion

In this research, hybrid power and desalinated water generation systems with two Multi-Effect Distillation (MED) technologies and Reverse Osmosis (RO) are investigated for a combined-cycle power plant in this study. The main finding of this research numbered below.

- By changing the combined cycle from power generation to a hybrid scheme of power and desalinated water, it was found that no change in the current system will reduce exergy efficiency from 51% to 48.8%.
- Most of the desalinated water produced is from the RO system.
- The result reveals that HRSG is not designed for the mentioned hybrid scheme.
- Economic studies showed that the final cost greatly depends on the design parameters.
- As a whole, the final cost was lower in the RO system than in MED because of more desalinated water produced in this part.
- For system optimization according to the genetic algorithm, the results showed that using 43 optimization parameters and imposing constraints like acidification temperature, the exergy efficiency was increased to 50%, and the cost was calculated to be 1.12 $/m3.

References

Al-Hallaj, S. *et al.* (2004) 'Conceptual design of a novel hybrid fuel cell/desalination system', *Desalination*. Elsevier, 164(1), pp. 19–31.

Ansari, K., Sayyaadi, H. and Amidpour, M. (2010) 'Thermoeconomic optimization of a hybrid pressurized water reactor (PWR) power plant coupled to a multi effect distillation desalination system with thermo-vapor compressor (MED-TVC)', *Energy*. Elsevier, 35(5), pp. 1981–1996.

Bejan, A. and Tsatsaronis, G. (1996) *Thermal design and optimization*. John Wiley & Sons.

Du, Y. *et al.* (2014) 'Multi-objective optimization of reverse osmosis networks by lexicographic optimization and augmented epsilon constraint method', *Desalination*. Elsevier, 333(1), pp. 66–81.

El-Nashar, A. M. (2001) 'Cogeneration for power and desalination—state of the art review', *Desalination*. Elsevier, 134(1–3), pp. 7–28.

Esfahani, I. J. *et al.* (2012) 'Modeling and genetic algorithm-based multi-objective optimization of the MED-TVC desalination system', *Desalination*. Elsevier, 292, pp. 87–104.

Esfahani, I. J. and Yoo, C. K. (2013) 'Exergy analysis and parametric optimization of three power and fresh water cogeneration systems using refrigeration chillers', *Energy*. Elsevier, 59, pp. 340–355.

Esmaeilzadehazimi, M. A. *et al.* (2021) 'Evaluation of a novel quadruple combined cycle with the magnetohydrodynamic generator based on 6E analysis', *Journal of Energy Resources Technology*. American

Society of Mechanical Engineers, 143(7), p. 72104.

Esmaieli, A. *et al.* (2013) 'Applying different optimization approaches to achieve optimal configuration of a dual pressure heat recovery steam generator', *International Journal of Energy Research*. Wiley Online Library, 37(12), pp. 1440–1452.

Ganapathy, V. (2002) *Industrial boilers and heat recovery steam generators: design, applications, and calculations*. CRC Press.

Ghiasi, M. *et al.* (2022) 'New Procedure for Optimal Integration of Steam Power Plant With Process Site Utility to Produce Power, Steam, and Freshwater', *Journal of Energy Resources Technology*. American Society of Mechanical Engineers, 144(10), p. 102103.

Gomar, Z., Heidary, H. and Davoudi, M. (2011) 'Techno-economics study to select optimum desalination plant for asalouyeh combined cycle power plant in iran', *World Academy of Science, Engineering and Technology*, 51.

Hosseini, S. R., Amidpour, M. and Shakib, S. E. (2012) 'Cost optimization of a combined power and water desalination plant with exergetic, environment and reliability consideration', *Desalination*. Elsevier, 285, pp. 123–130.

Kamali, R. K. *et al.* (2008) 'Thermodynamic design and parametric study of MED-TVC', *Desalination*. Elsevier, 222(1–3), pp. 596–604.

Kamali, R. K. and Mohebinia, S. (2008) 'Experience of design and optimization of multi-effects desalination systems in Iran', *Desalination*. Elsevier, 222(1–3), pp. 639–645.

Kaviri, A. G., Jaafar, M. N. M. and Lazim, T. M. (2012) 'Modeling and multi-objective exergy based optimization of a combined cycle power plant using a genetic algorithm', *Energy Conversion and Management*. Elsevier, 58, pp. 94–103.

Khoshgoftar Manesh, M. H. *et al.* (2021) 'Dynamic Advanced Exergetic, Exergoeconomic, and Environmental Analyses of a Hybrid Solar City Gate Station', *Journal of Energy Resources Technology*. American Society of Mechanical Engineers, 143(10), p. 102105.

Lefebvre, A. H. and Ballal, D. R. (2010) *Gas turbine combustion: alternative fuels and emissions*. CRC press.

Lisbona, P., Uche, J. and Serra, L. (2005) 'High-temperature fuel cells for fresh water production', *Desalination*. Elsevier, 182(1–3), pp. 471–482.

Manesh, M. H. K. *et al.* (2013) 'Optimal coupling of site utility steam network with MED-RO desalination through total site analysis and exergoeconomic optimization', *Desalination*. Elsevier, 316, pp. 42–52.

Mokhtari, H., Ahmadisedigh, H. and Ameri, M. (2017) 'The optimal design and 4E analysis of double pressure HRSG utilizing steam injection for Damavand power plant', *Energy*. Elsevier, 118, pp. 399–413.

Mokhtari, H., Ahmadisedigh, H. and Ebrahimi, I. (2016) 'Comparative 4E analysis for solar desalinated water production by utilizing organic fluid and water', *Desalination*. Elsevier, 377, pp. 108–122.

Mokhtari, H., Bidi, M. and Gholinejad, M. (2014) 'Thermoeconomic analysis and multiobjective optimization of a solar desalination plant', *Journal of solar energy*. Hindawi, 2014.

Mokhtari, H., Esmaieli, A. and Hajabdollahi, H. (2016) 'Thermo-economic analysis and multiobjective optimization of dual pressure combined cycle power plant with supplementary firing', *Heat Transfer—Asian Research*. Wiley Online Library, 45(1), pp. 59–84.

Najafi, B. *et al.* (2014) 'Exergetic, economic and environmental analyses and multi-objective optimization of an SOFC-gas turbine hybrid cycle coupled with an MSF desalination system', *Desalination*. Elsevier, 334(1), pp. 46–59.

Rahimi, M. J. and Alibabaee, H. (2021) 'Energy and Environmental Comparison of Different Scenarios for Cogeneration of Power and Desalinated Water in Iran', *Gas Processing Journal*. University of Isfahan, 9(1), pp. 29–42.

El Saie, M. H. A., El Saie, Y. M. H. A. and El Gabry, H. (2003) 'Techno-economic study for combined cycle power generation with desalination plants at Sharm El Sheikh', *Desalination*. Elsevier, 153(1–3), pp. 191–198.

Salehi, G. R., Ahmadpour, M. and Khoshnazar, H. (2011) 'Modeling of the seawater greenhouse systems', in *World Renewable Energy Congress-Sweden; 8-13 May; 2011; Linköping; Sweden*. Linköping University Electronic Press, pp. 3733–3740.

Sayyaadi, H., Saffari, A. and Mahmoodian, A. (2010) 'Various approaches in optimization of multi effects distillation desalination systems using a hybrid meta-heuristic optimization tool', *Desalination*. Elsevier, 254(1–3), pp. 138–148.

Seckin, C. (2020) 'Effect of Operational Parameters on a Novel Combined Cycle of Ejector Refrigeration Cycle and Kalina Cycle', *Journal of Energy Resources Technology*. American Society of Mechanical Engineers Digital Collection, 142(1).

Shahandeh, H., Ivakpour, J. and Kasiri, N. (2014) 'Internal and external HIDiCs (heat-integrated distillation columns) optimization by genetic algorithm', *Energy*. Elsevier, 64, pp. 875–886.

Shenvi, S. S., Isloor, A. M. and Ismail, A. F. (2015) 'A review on RO membrane technology: Developments and challenges', *Desalination*. Elsevier, 368, pp. 10–26.

Silva, R. *et al.* (2014) 'Thermo-economic design optimization of parabolic trough solar plants for industrial process heat applications with memetic algorithms', *Applied Energy*. Elsevier, 113, pp. 603–614.

Skiborowski, M. *et al.* (2012) 'Model-based structural optimization of seawater desalination plants', *Desalination*. Elsevier, 292, pp. 30–44.

Vazini Modabber, H. and Khoshgoftar Manesh, M. H. (2019) 'Exergetic, Exergoeconomic and Exergoenvironmental Multi-Objective Genetic Algorithm Optimization of Qeshm Power and Water Cogeneration Plant', *Gas Processing Journal*. University of Isfahan, 7(2), pp. 1–28.